Supplementary Information (SI) for Reaction Chemistry & Engineering.

SUPPORTING INFORMATION

Kinetic and Mechanistic Studies of Cyclohexane Oxidation with tert-Butyl hydroperoxide over M-N_4 Catalysts

Ethan P. Iaia,[1] Miles G. Miller,[1] Ademola Soyemi,[1] Martin G. Bakker,[2] Tibor Szilvási,[1] James W. Harris[1*]

1. Department of Chemical and Biological Engineering, The University of Alabama, Tuscaloosa, AL, 35487
2. Department of Chemistry and Biochemistry, The University of Alabama, Tuscaloosa, AL, 35487

*Corresponding author: james.harris@eng.ua.edu

Table of Contents

S.1 Carbon Balance

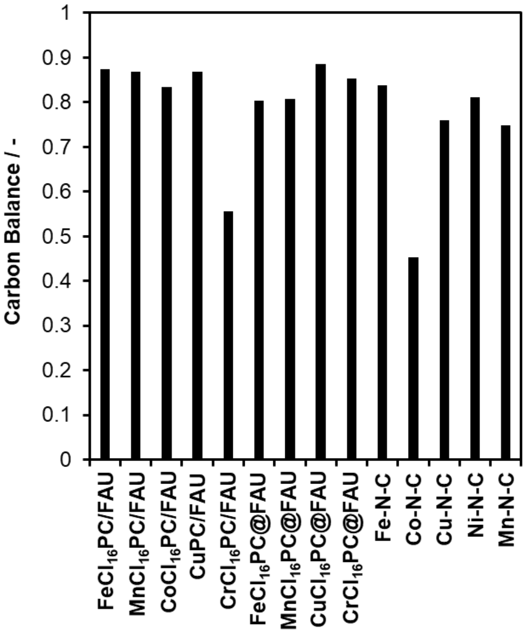

Figure S.1. Carbon balance for data reported in Figure 7. Reaction conditions: acetonitrile solvent, 1.05 M cyclohexane, 0.52 M TBHP, 303 K, 350 RPM, 0.020 g_{cat}, 1.8 ks.

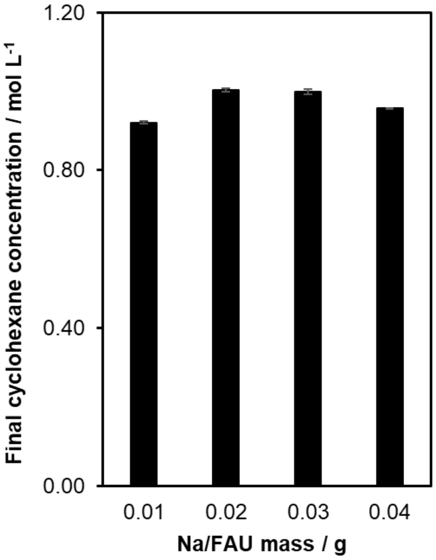

Figure S.2. Measured concentration of cyclohexane after stirring the given mass of Na/FAU in 4 cm^3 of 1.05 mol dm^{-3} cyclohexane in acetonitrile for 1.8 ks at 303 K.

S.2 Additional XRD

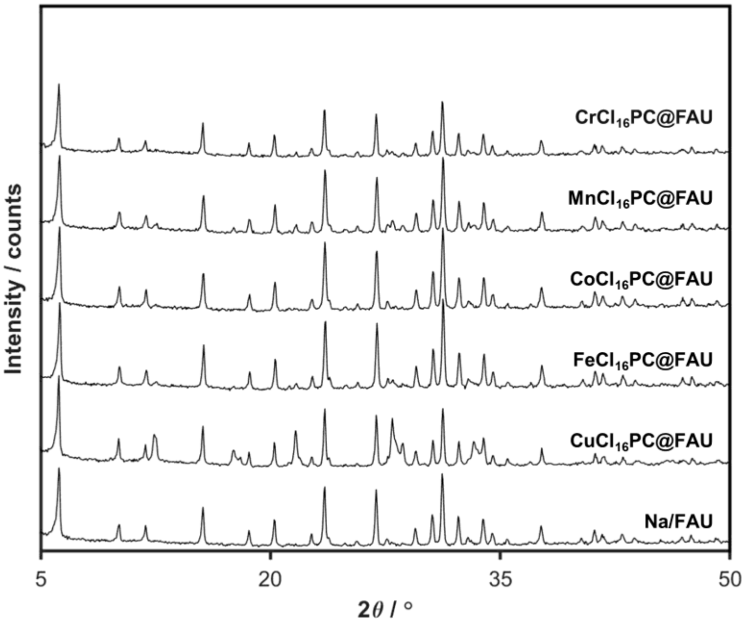

Figure S.3. XRD patterns for various FAU and MPC@FAU samples.

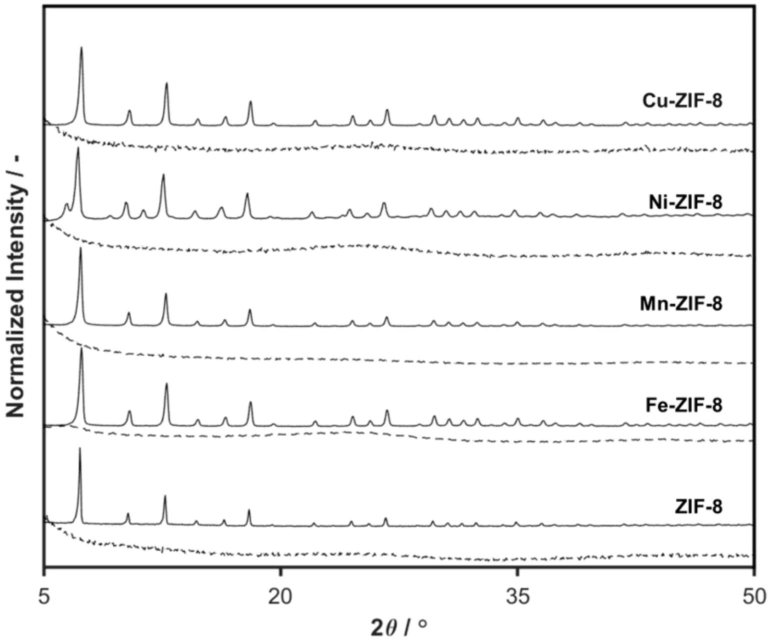

Figure S.4. XRD patterns for various ZIF-8 samples before (solid) and after (dashed) pyrolysis.

S.3 SEM and TEM Images

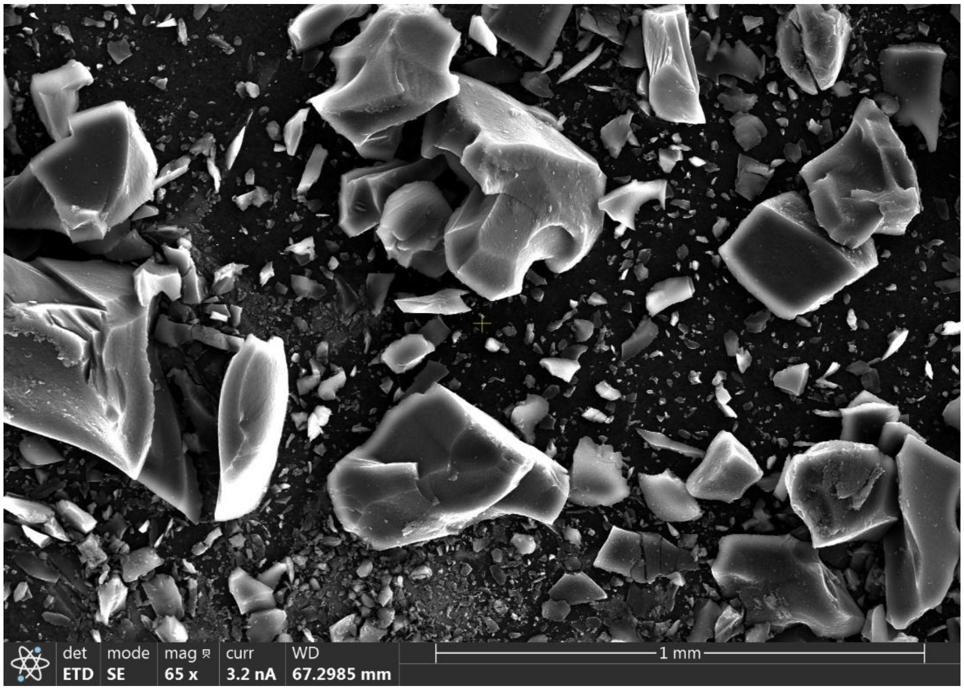

Figure S.5. SEM image of Ni-N-C used to determine Ni loading by EDX.

Table S.1. Elemental analysis of Ni-N-C evaluated by SEM-EDX. Wt% values are the average of six different areas in Figure S.5.

Element	Wt%	Standard Deviation
C	86	2.3
N	2.0	1.8
O	9.7	1.1
Ni	1.4	0.3
Fe	0.7	0.3

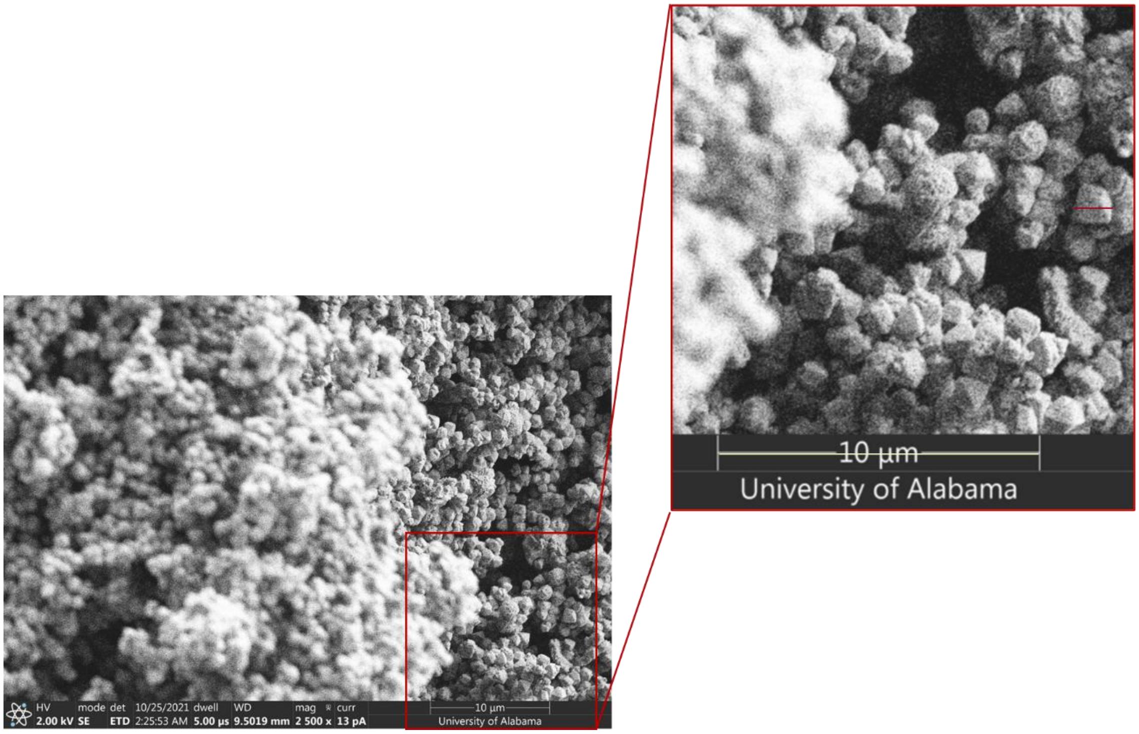

Figure S.6. SEM image of $CuCl_{16}PC@FAU$. Red line in insert along with yellow line on scale were used to determine particle diameter for Weisz-Prater criterion calculations.

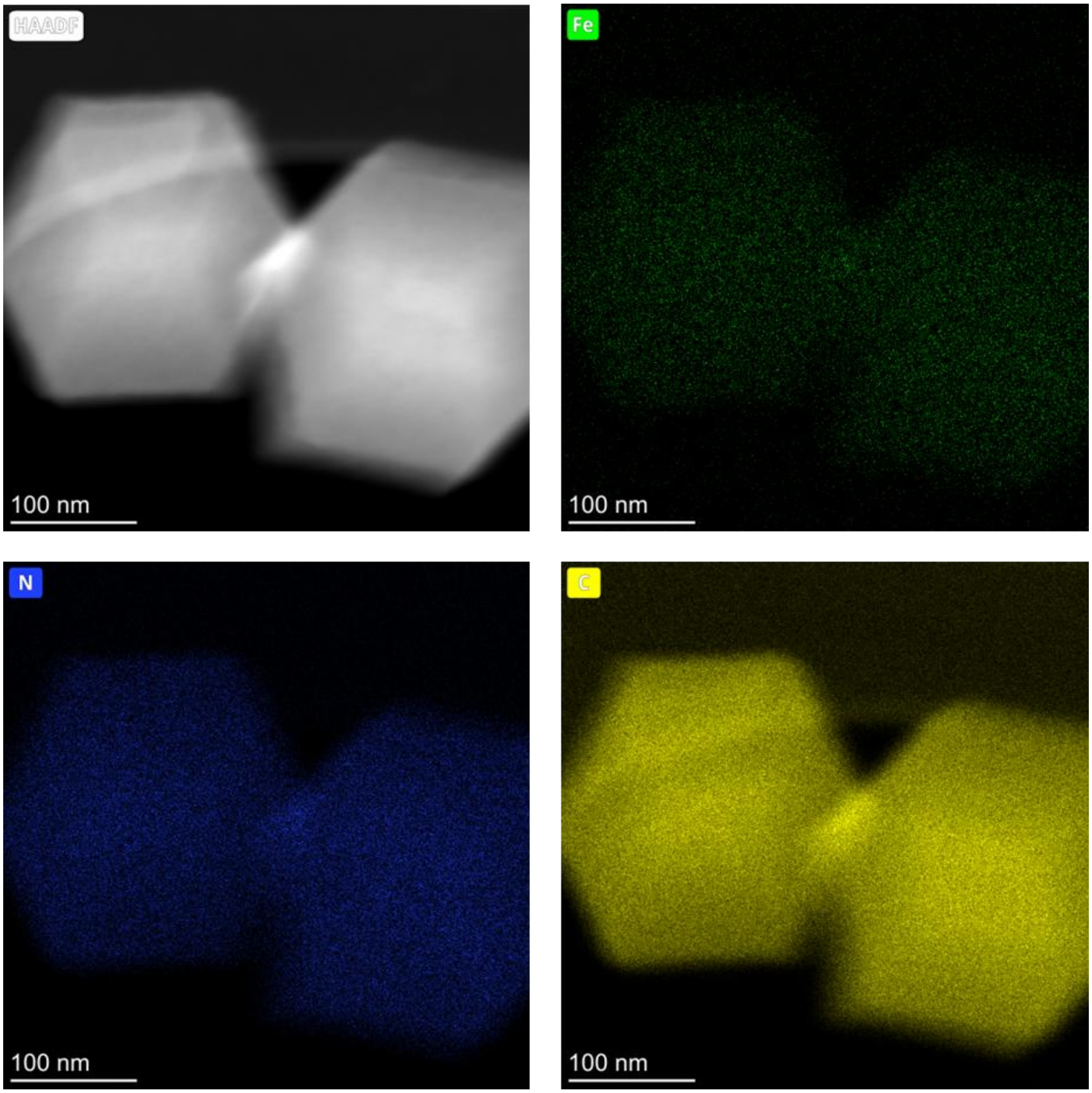

Figure S.7. TEM image of Fe-N-C with EDX maps for Fe, N, and C.

S.4 Nitrogen Adsorption Isotherms

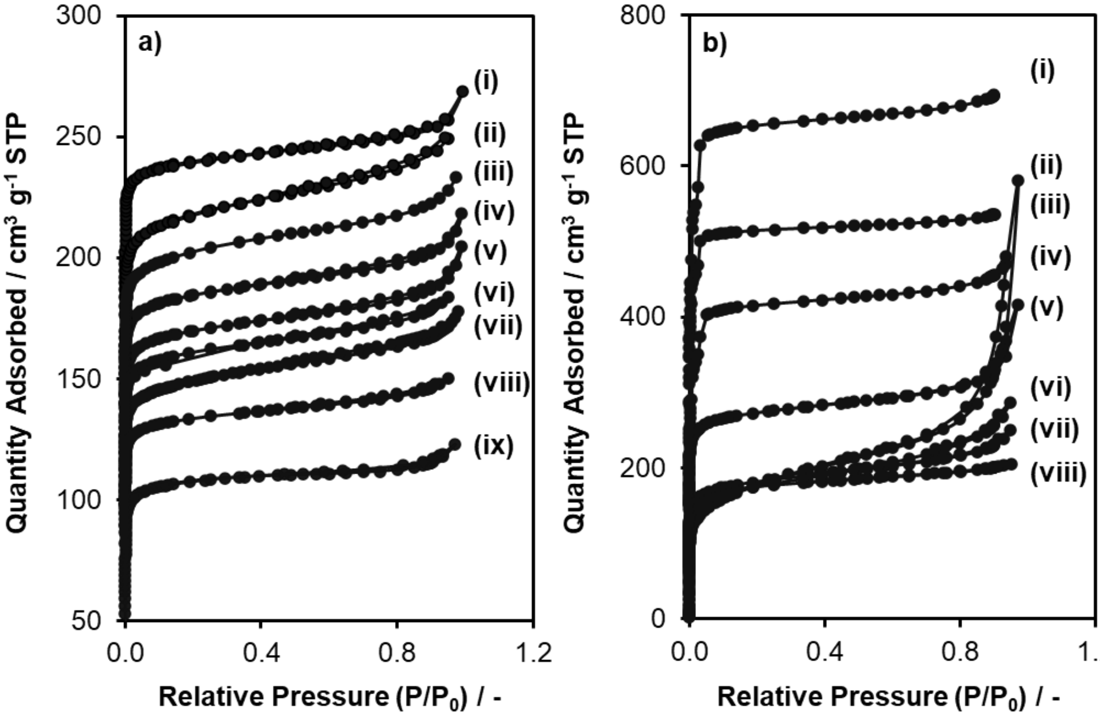

Figure S.8. N_2 physisorption isotherms for various (a) Na/FAU, MPC/FAU and MPC@FAU samples: (i) Na/FAU, (ii) $CrClCl_{16}$/FAU, (iii) $MnCl_{16}$PC@FAU offset by 35, (iv) $CuCl_{16}$PC/FAU, (v) $FeCl_{16}$PC/FAU, (vi) $CoCl_{16}$PC@FAU, (vii) $CoCl_{16}$PC/FAU, (viii) $CuCl_{16}$PC@FAU, and (ix) $FeCl_{16}$PC@FAU offset by -50; (b) M-N-C and M-ZIF-8 samples: (i) Mn-ZIF-8, (ii) Co-N-C, (iii) Fe-ZIF-8 offset by 150, (iv) Ni-ZIF-8, (v) Ni-N-C offset by 75, (vi) Cu-N-C, (vii) Mn-N-C, and (vii) Fe-N-C.

S.5 DRUV Spectra

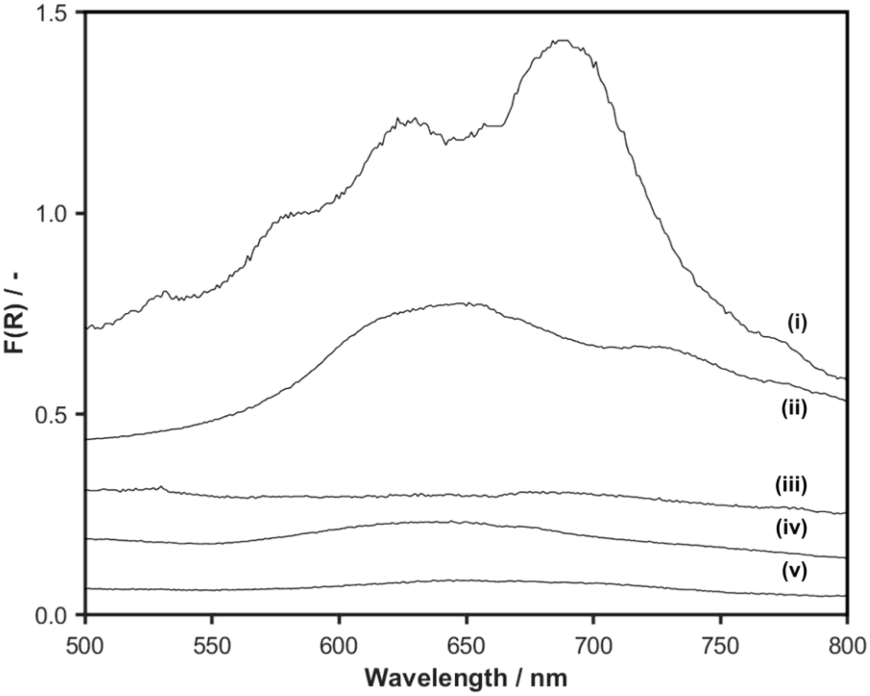

Figure S.9. DRUV spectra in Kubelka-Munk Units of (i) $FeCl_{16}PC@FAU$ offset by 0.15, (ii) $CuCl_{16}PC@FAU$ offset by 0.4, (iii) $CoCl_{16}PC@FAU$, (iv) $MnCl_{16}PC@FAU$ offset vertically by 0.1, (v) $CrCl_{16}PC@FAU$.

S.6 X-ray Absorption Spectra

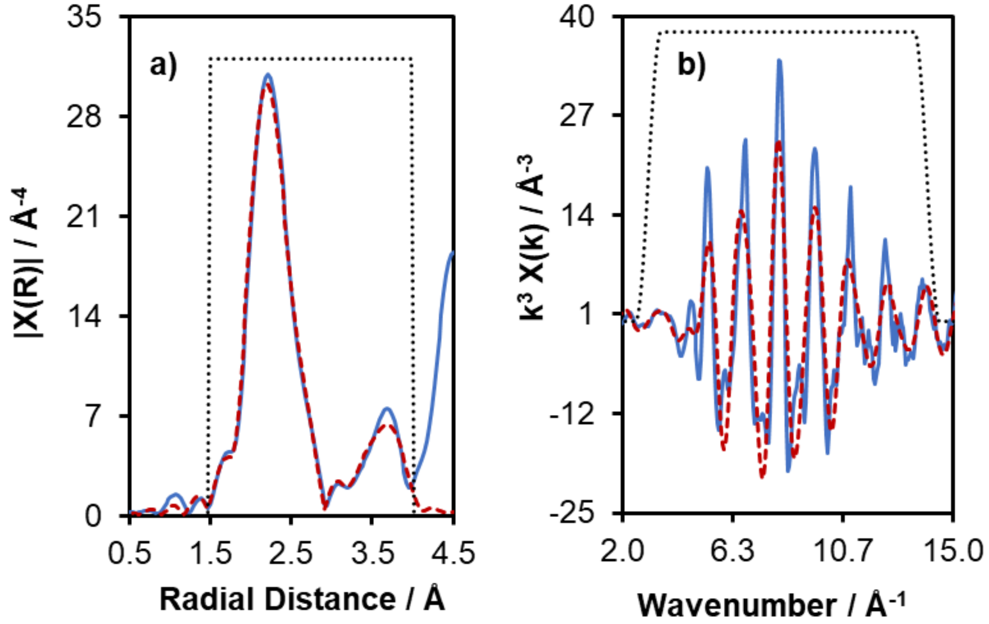

Figure S.10. *Ex situ* Fourier-transform EXAFS of Fe foil (solid blue), fit used to determine amplitude reduction factor (red dash), and fitting window (black dots) plotted in a) R space and b) k space. K range: 3-14.

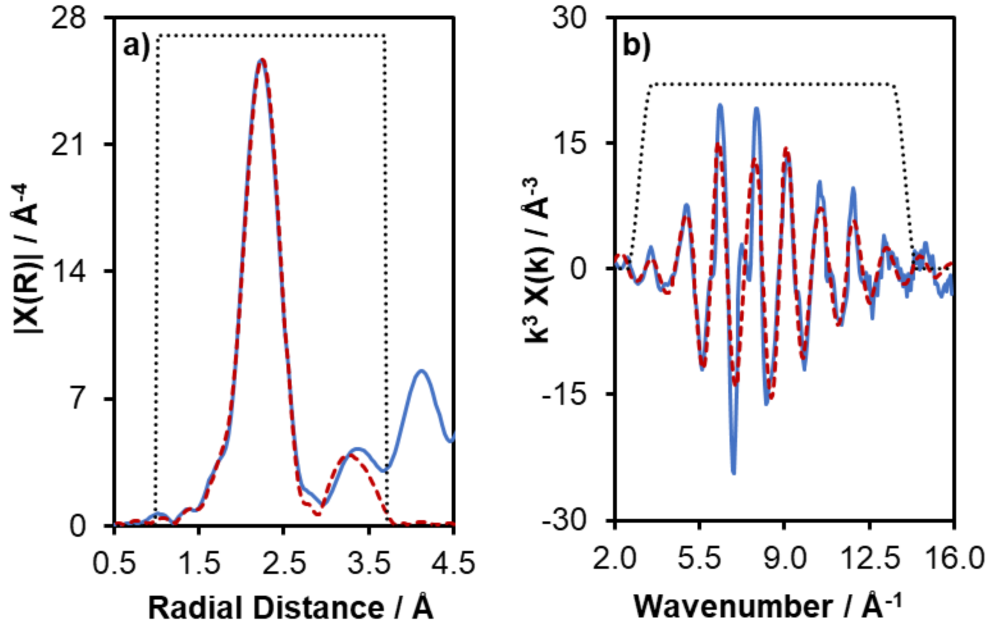

Figure S.11. *Ex situ* Fourier-transform EXAFS of Cu foil (solid blue), fit used to determine amplitude reduction factor (red dash), and fitting window (black dots) plotted in a) R space and b) k space. K range: 3-14.

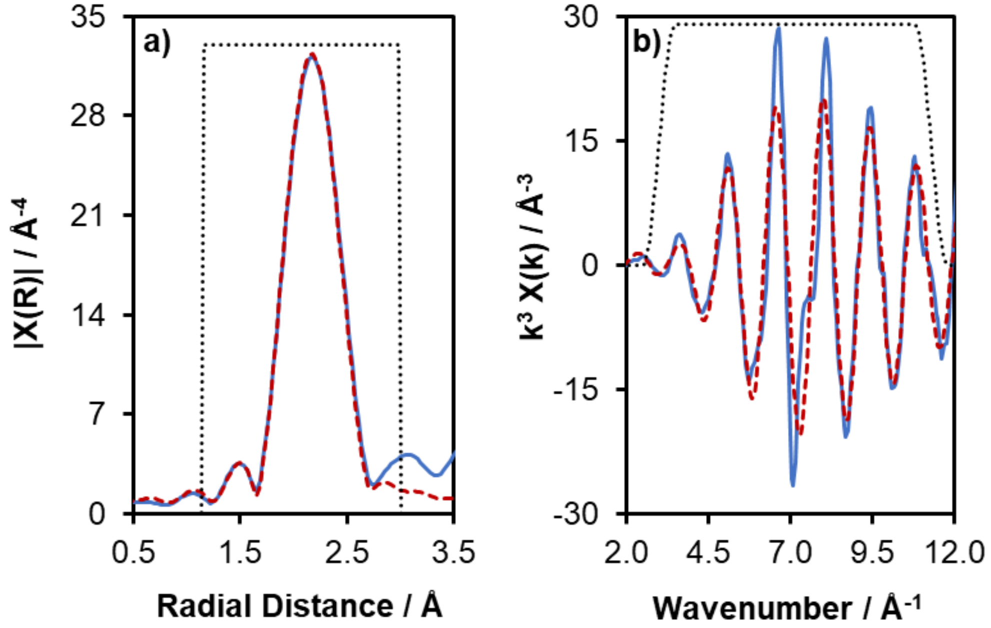

Figure S.12. *ex situ* Fourier-transform EXAFS of Co foil (solid blue), fit used to determine amplitude reduction factor (red dash), and fitting window (black dots) plotted in a) R space and b) k space. K range: 3-11.3.

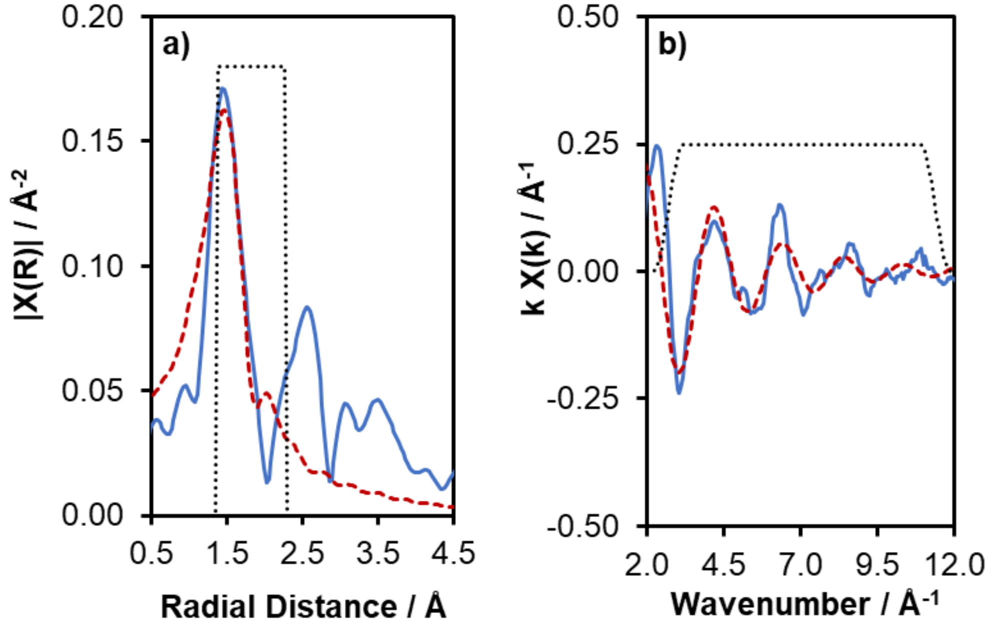

Figure S.13. *Ex situ* Fourier-transform EXAFS of $FeCl_{16}PC@FAU$ (solid blue), fit used to determine coordination numbers and bond distances (red dash), and fitting window (black dots) plotted in a) R space and b) k space. K range: 2.7-11.4.

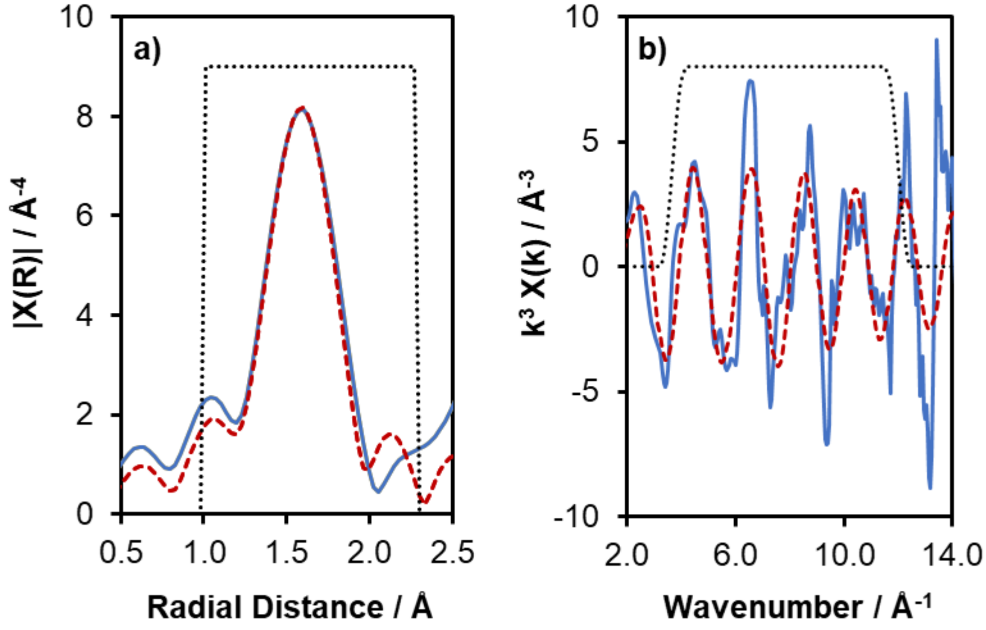

Figure S.14. *Ex situ* Fourier-transform EXAFS of $CuCl_{16}PC@FAU$ (solid blue), fit used to determine coordination numbers and bond distances (red dash), and fitting window (black dots) plotted in a) R space and b) k space. K range: 3.7-12.

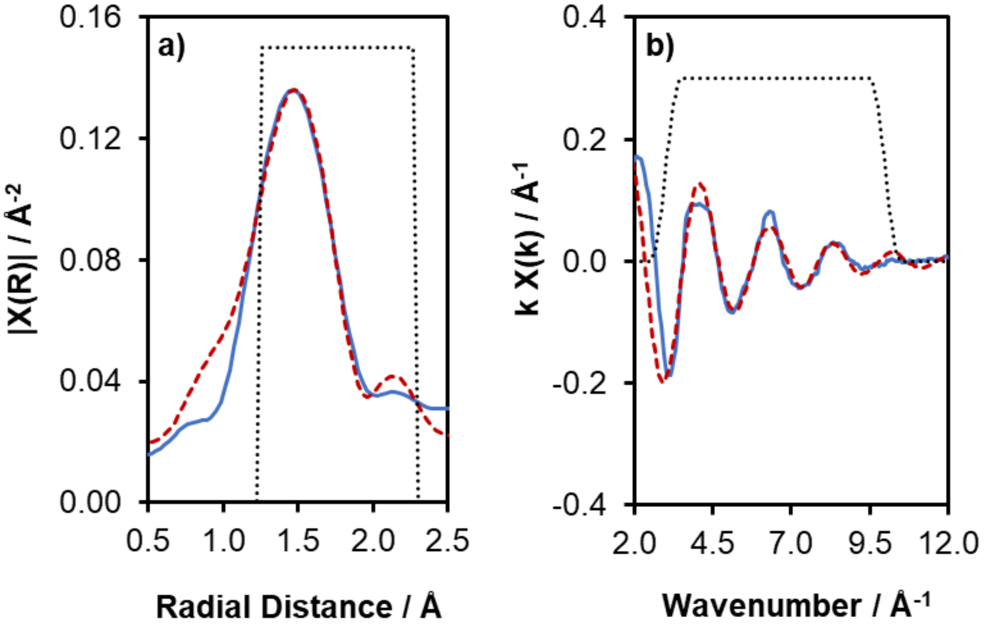

Figure S.15. *Ex situ* Fourier-transform EXAFS of Fe-N-C (solid blue), fit used to determine coordination numbers and bond distances (red dash), and fitting window (black dots) plotted in a) R space and b) k space. K range: 3-10.

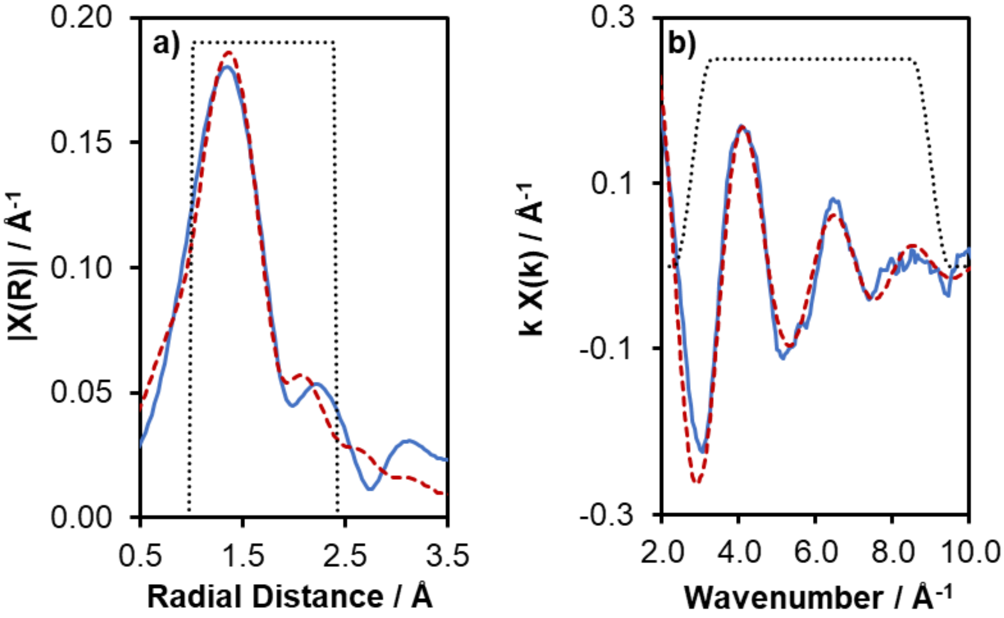

Figure S.16. *Ex situ* Fourier-transform EXAFS of Cu-N-C (solid blue), fit used to determine coordination numbers and bond distances (red dash), and fitting window (black dots) plotted in a) R space and b) k space. K range: 2.8-9.

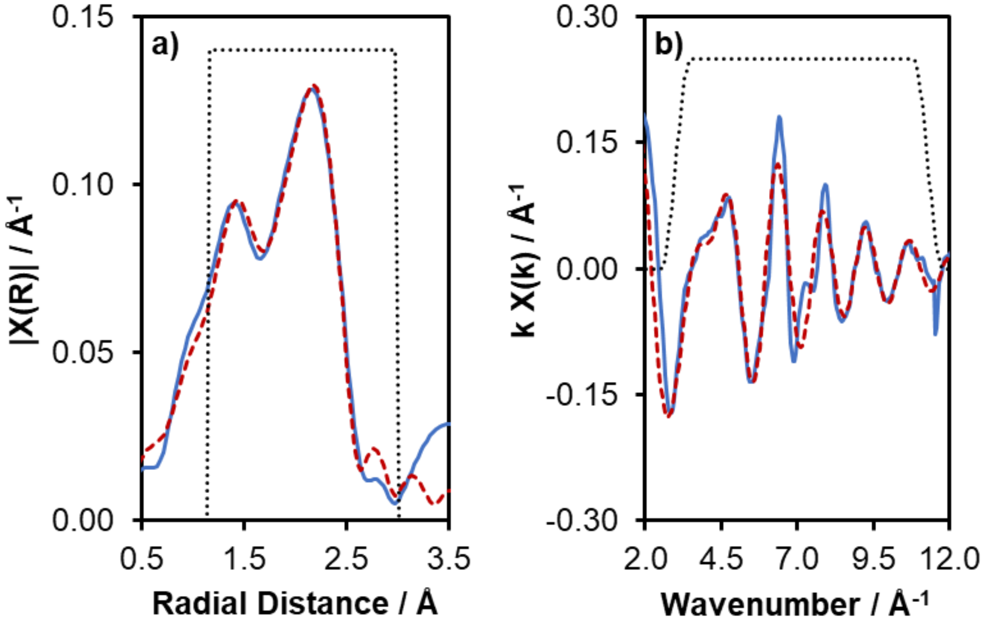

Figure S.17. *Ex situ* Fourier-transform EXAFS of Co-N-C (solid blue), fit used to determine coordination numbers and bond distances (red dash), and fitting window (black dots) plotted in a) R space and b) k space. K range: 3-11.3.

S.7 Tests for Mass Transfer Limitations

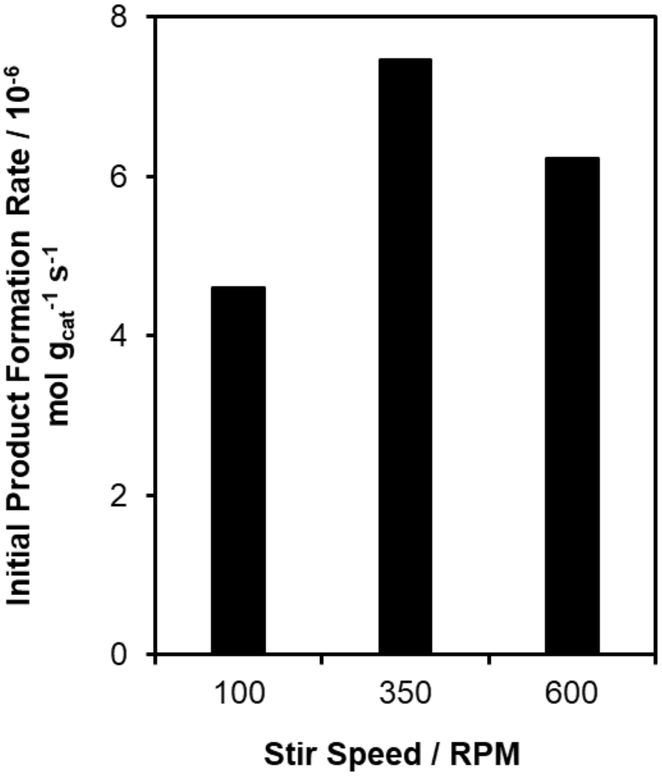

Figure S.18. Initial combined product formation rate measured over Fe-N-C at varied stir speeds. Reaction conditions: acetonitrile solvent, 1.05 M cyclohexane, 0.52 M TBHP, 303 K, 0.010 g_{cat}, 0.15 ks.

The impact of internal mass transfer limitations was evaluated on the basis of Weisz-Prater criterion.[1] The Thiele modulus, Φ, can be calculated using equation S.1, where r_A is the observed initial product formation rate normalized per kg of catalyst, ρ_c is the crystallite density in kg m^{-3}, R is the crystallite radius in m, C_{AS} is the concentration of cyclohexane in kmol m^{-3}, and D_e is the effective diffusivity of cyclohexane in acetonitrile.

$$\Phi = \sqrt{\frac{-r_A \rho_S R^2}{D_e C_{AS}}} \tag{S.1}$$

Using CuCl16PC@FAU, $r_A = 1.37 \times 10^{-8}$ kmol kg_{cat} s^{-1}, $\rho_c = 825$ kg m^3 for NaY from,[2] $R = 6.2 \times 10^{-7}$ from SEM images (See Section S.3), $D_e = 2.3 \times 10^{-10}$ m^2 s^{-1} for cyclohexane in porous silica,[3] and $C_{AS} = 1.05$ kmol m^{-3}, Φ is estimated to be 1.3×10^{-4}, which is < 1, so it can be assumed that internal mass transfer limitations are negligible.[4]

S.8 Additional Control Experiments

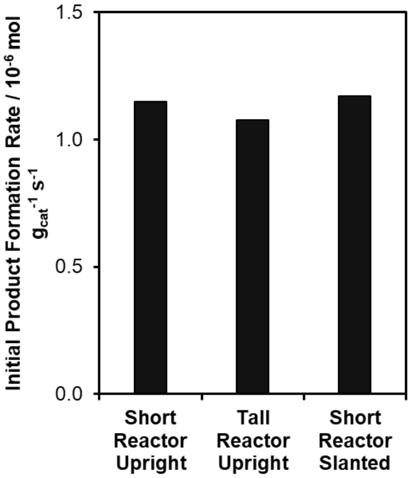

Figure S.19. Initial combined product formation rate measured over $MnCl_{16}PC/FAU$ in different sized reactors held upright or slanted ~45°. Reaction conditions: acetonitrile solvent, 1.05 M cyclohexane, 0.52 M TBHP, 303 K, 0.010 g_{cat}, 1.8 ks.

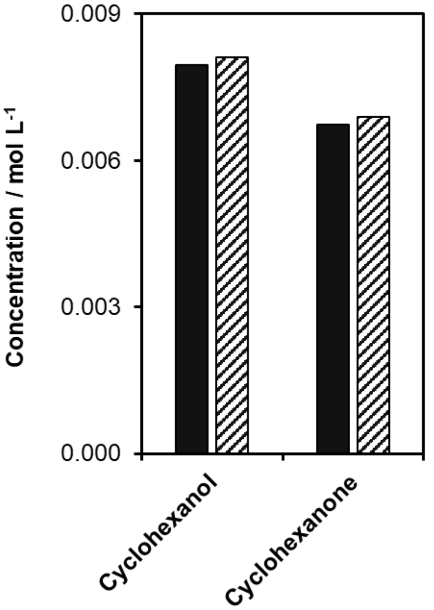

Figure S.20. Concentration of cyclohexanol and cyclohexanone after cyclohexane oxidation batch reaction with Fe-N-C (filled bars) and after filtering out catalyst and stirring for an additional 1.8 ks. Reaction conditions: acetonitrile solvent, 1.05 M cyclohexane, 0.52 M TBHP, 303 K, 0.010 g_{cat}, 0.15 ks.

S.9 Batch Time Data

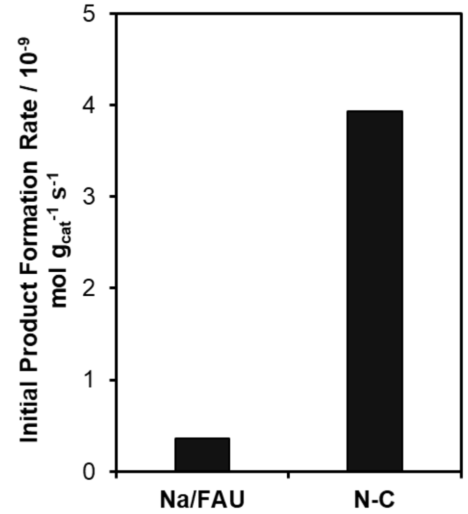

Figure S.21. Initial combined product formation rate measured over Na/FAU and N-C. Reaction conditions: acetonitrile solvent, 1.05 M cyclohexane, 0.52 M TBHP, 303 K, 0.010 g_{cat}, 1.8 ks.

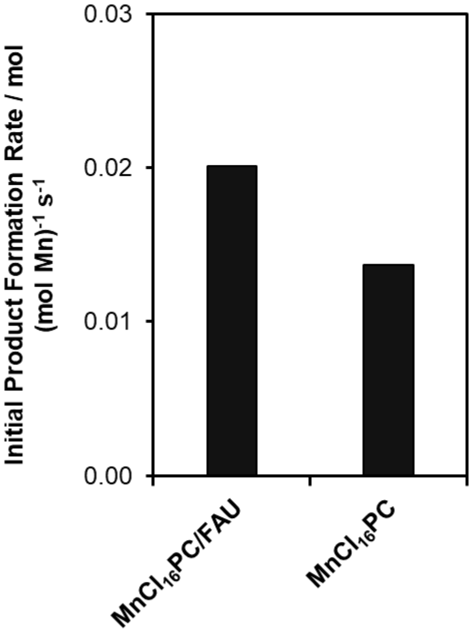

Figure S.22. Initial combined product formation rate measured over $MnCl_{16}PC/FAU$ and $MnCl_{16}PC$. Reaction conditions: acetonitrile solvent, 1.05 M cyclohexane, 0.52 M TBHP, 303 K, 0.010 g_{cat}, 1.8 ks.

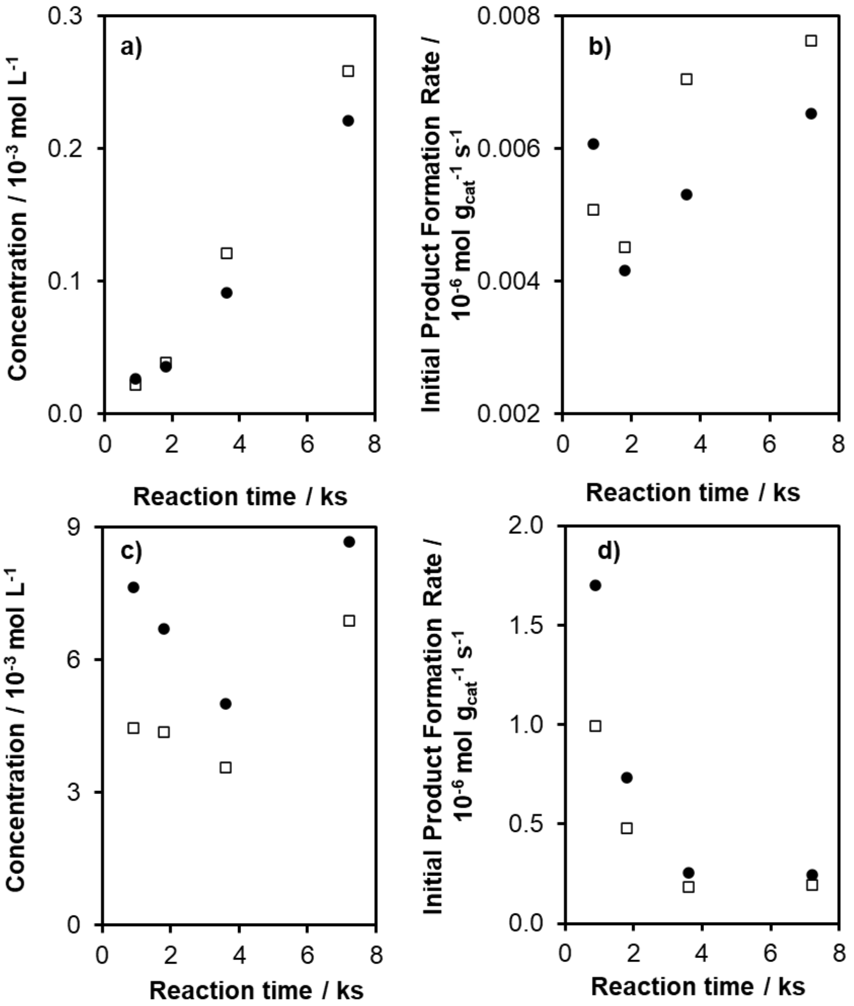

Figure S.23. a) concentrations and b) gravimetric formation rates of cyclohexanol (filled circles) and cyclohexanone (open squares) during cyclohexane oxidation with $CuCl_{16}PC@FAU$. c) concentrations and d) gravimetric formation rates of cyclohexanol (filled circles) and cyclohexanone (open squares) during cyclohexane oxidation with $CuF_{16}PC/FAU$. Reaction conditions: acetonitrile solvent, 1.05 M cyclohexane, 0.52 M TBHP, 333 K, 350 RPM, 0.020 g_{cat}.

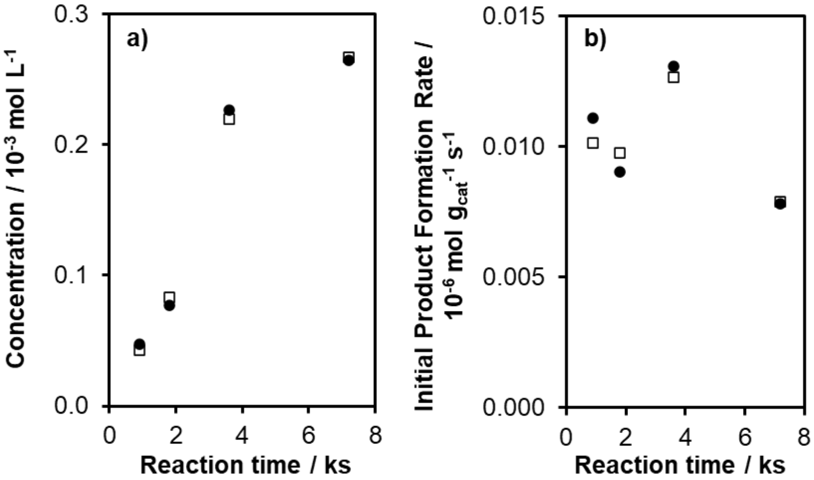

Figure S.24. a) concentrations and b) gravimetric formation rates of cyclohexanol (filled circles) and cyclohexanone (open squares) during cyclohexane oxidation with $CoCl_{16}PC/FAU$. Reaction conditions: acetonitrile solvent, 1.05 M cyclohexane, 0.52 M TBHP, 303 K, 350 RPM, 0.020 g_{cat}.

S.10 Rate Expression Derivations

Mechanism from Parton et al.[5]

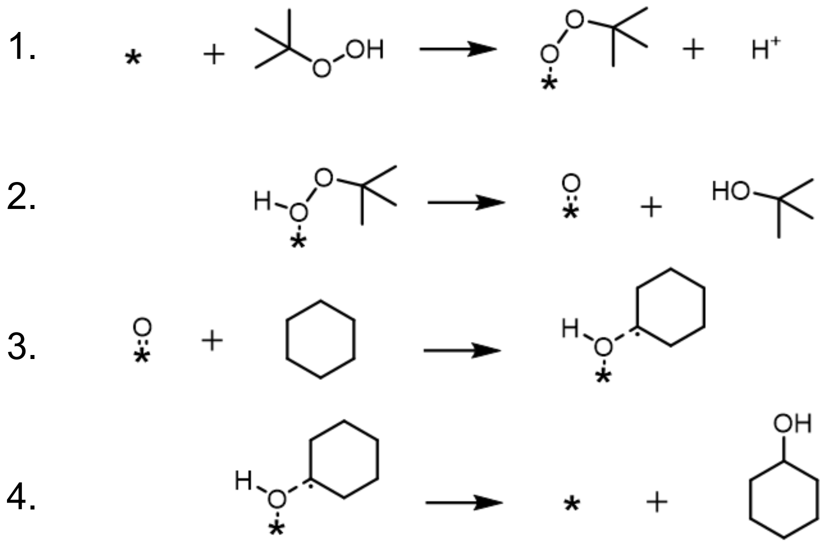

Scheme S.1 Cyclohexane oxidation mechanism with TBHP as proposed by Parton and coworkers.[5]

This mechanism was first proposed by Parton and coworkers.[5] Kinetic isotope effect (KIE) experiments suggest that hydrogen abstraction by the active metal-oxo species is the rate limiting step, meaning the overall rate can be expressed as equation S.2.[5]

$$r_{net} = k_3[\text{cyclohexane}][*{=}\,\text{O}] \tag{S.2}$$

This can be simplified by applying the pseudo-steady-state hypothesis to solve for [∗=O], yielding equation S.3.

$$r_2 = r_3$$

$$k_2[*-\text{OOtBu}][\text{H}^+] = k_3[*{=}\,\text{O}][\text{cyclohexane}]$$

$$[*{=}\,\text{O}] = \frac{k_2[*-\text{OOtBu}][\text{H}^+]}{k_3[\text{cyclohexane}]} \tag{S.3}$$

Equation S.3 can be further simplified by applying the pseudo-steady-state hypothesis to [∗−OOtBu], leading to equation S.4.

$$r_1 = r_2$$

$$k_1[*][\text{TBHP}] = k_2[*-\text{OOtBu}][\text{H}^+]$$

$$[*-\text{OOtBu}] = \frac{k_1[*][\text{TBHP}]}{[\text{H}^+]} \tag{S.4}$$

Inserting equation S.4 into equation S.3 yields equation S.5.

$$[*=\mathrm{O}] = \frac{k_2 k_1 [*][\mathrm{TBHP}]}{k_3[\mathrm{cyclohexane}]} \tag{S.5}$$

Plugging equation 5 into equation S.2 yields equation S.6.

$$r_{net} = k_2 k_1 [*][\mathrm{TBHP}] \tag{S.6}$$

The site balance can be defined using equation S.7.

$$[L] = [*] + [*=\mathrm{O}] + [* - \mathrm{OOtBu}] \tag{S.7}$$

Dividing equation S.6 by equation S.7 gives the final rate expression.

$$\frac{r_{net}}{[L]} = \frac{k_2 k_1 [\mathrm{TBHP}]}{1 + \frac{k_2 k_1 [\mathrm{TBHP}]}{k_3[\mathrm{cyclohexane}]}} \tag{S.8}$$

Langmuir-Hinshelwood Mechanism from Becerra et al.[6]

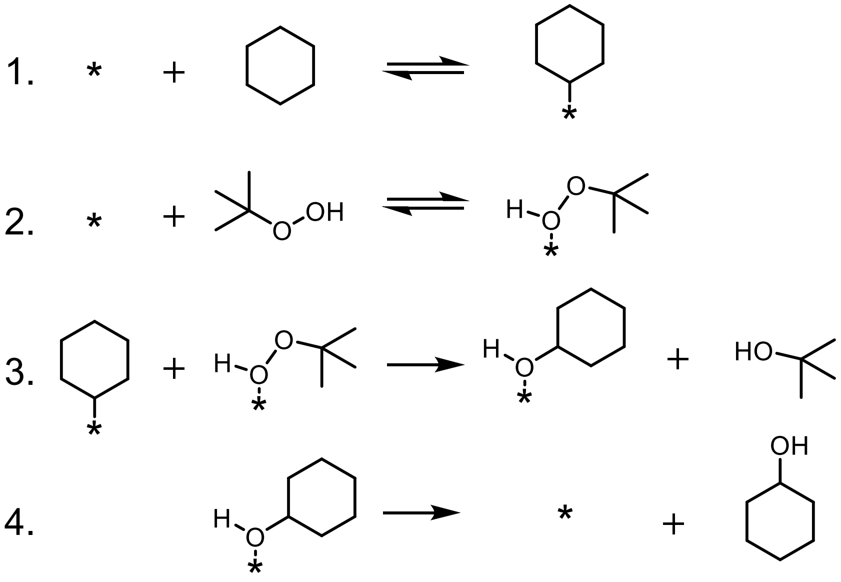

Scheme S.2 Proposed cyclohexane oxidation mechanism with TBHP as proposed modified from Beccera and coworkers.[6]

This mechanism was modified from a previously proposed mechanism by Becerra and coworkers[6] for the oxidation of α-pinene with TBHP over $\mathrm{FeCl_{16}PC/SiO_2}$. Assuming that the third step where the adsorbed species react is the rate determining step, the overall rate can be expressed as equation S.9.

$$r_{net} = k_3 [*=\mathrm{O}][* - \mathrm{OOtBu}] \tag{S.9}$$

This can be simplified by assuming that the reactant adsorption steps (steps 1 and 2) are quasi-equilibrated, leading to equations S.10 and S.11, respectively.

$$r_1 = r_{-1}$$

$$k_1[*][\text{cyclohexane}] = k_{-1}[*=\text{O}]$$

$$[*=\text{O}] = K_1[*][\text{cyclohexane}] \tag{S.10}$$

$$r_2 = r_{-2}$$

$$k_2[*][\text{TBHP}] = k_{-2}[*-\text{OOtBu}]$$

$$[*-\text{OOtBu}] = K_2[*][\text{TBHP}] \tag{S.11}$$

Inserting equations S.10 and S.11 into equation S.9 yields equation S.12.

$$r_{net} = k_3 K_1 K_2 [*]^2 [\text{cyclohexane}][TBHP] \tag{S.12}$$

Dividing equation S.12 by the site balance (equation S.7) leads to the final rate expression.

$$\frac{r_{net}}{[L]} = \frac{k_3 K_1 K_2 [\text{cyclohexane}][\text{TBHP}]}{(1+K_2[TBHP]+K_1[cyclohexane])^2} \tag{S.13}$$

S.11 Parity and Residual Plots

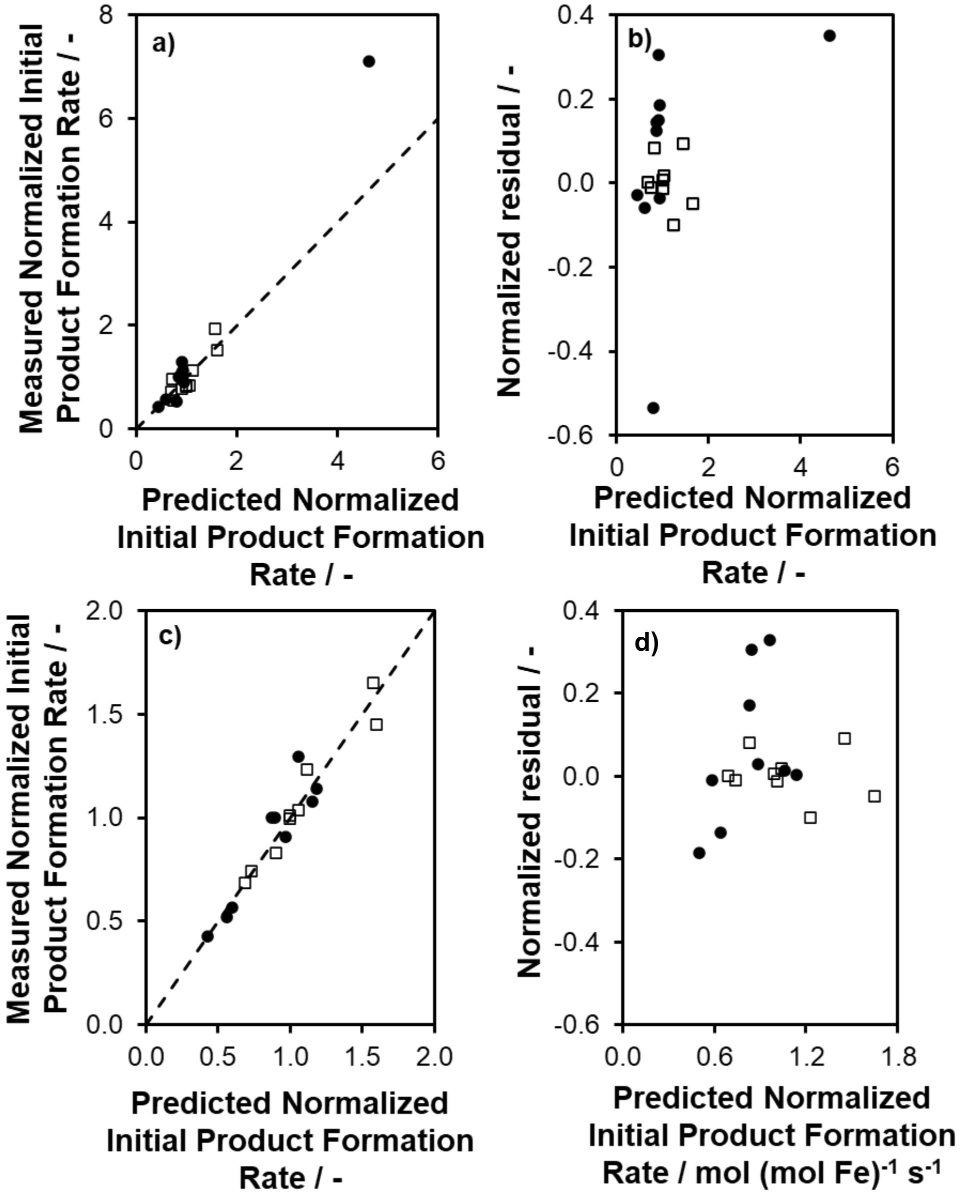

Figure S.25. a) Parity and b) normalized residual plots comparing measured initial rates to rates predicted by model proposed by Parton and coworkers,[5] over $FeCl_{16}PC@FAU$ (filled circles) and Fe-N-C (open squares). c) Parity and d) normalized residual plots when data collected in pure cyclohexane is excluded. Reaction conditions: acetonitrile solvent, 0.5-1.15 M cyclohexane, 0.17-1.05 M TBHP, 303 K, 350 RPM, 0.15 or 1.8 ks.

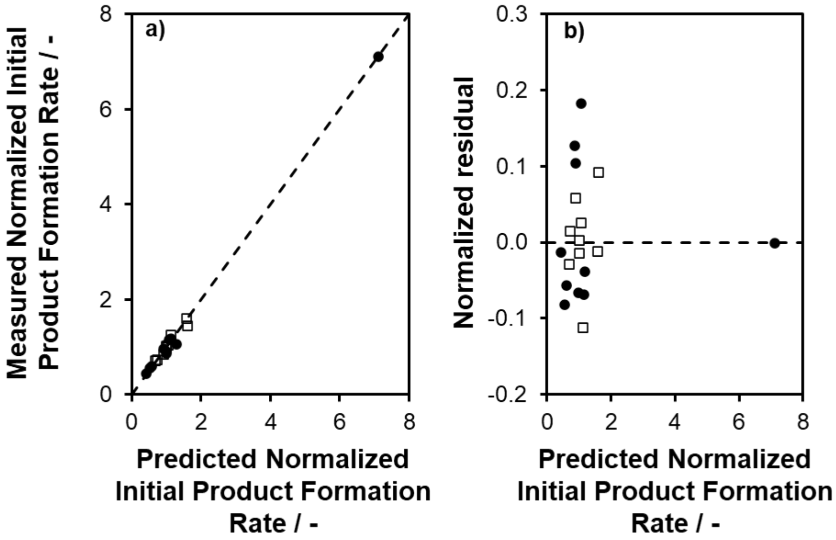

Figure S.26. a) Parity and b) normalized residual plots comparing measured initial rates to rates predicted by Langmuir-Hinshelwood mechanism modified from Beccera and coworkers,[6] over $FeCl_{16}PC@FAU$ (filled circles) and Fe-N-C (open squares). Reaction conditions: acetonitrile solvent, 0.5-1.15 M cyclohexane, 0.17-1.05 M TBHP, 303 K, 350 RPM, 0.15 or 1.8 ks.

S.12 Additional Kinetic Data

Table S.2. Cumulative turnover numbers. Reaction conditions: acetonitrile solvent, 1.05 M cyclohexane, 0.52 M TBHP, 303 K, 350 RPM, 0.020 g_{cat}, 1.8 ks.

Sample	**TON**
$FeCl_{16}PC/FAU$	120
$MnCl_{16}PC/FAU$	22
$CoCl_{16}PC/FAU$	1.4
CuPC/FAU	0.03
$CrCl_{16}PC/FAU$	0.02
$FeCl_{16}PC@FAU$	7.0
$MnCl_{16}PC@FAU$	2.1
$CuCl_{16}PC@FAU$	9.2
$CrCl_{16}PC@FAU$	0.23
Fe-N-C	100
Co-N-C	10

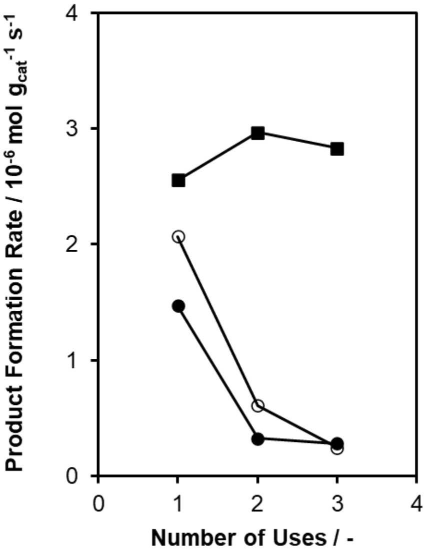

Figure S.27. Initial combined product formation rate measured over $FeCl_{16}PC@FAU$ (filled circles), $FeCl_{16}PC/FAU$ (open circles), and Fe-N-C (filled squares) after the first, second, and third use of the same loading of catalyst. Reaction conditions: acetonitrile solvent, 1.4 M cyclohexane, 0.52 M TBHP, 303 K, 350 RPM, 0.020 g_{cat}.

S.13 Full Microkinetic Model

Table S.3. List of elementary reaction steps, reaction free energies (ΔG), activation Gibbs free energies ($\Delta G^{\ddagger 0}$) and rate constants (k) accounted for in the microkinetic model shown in **Scheme 4**.

Step Number	Elementary step	ΔG (kJ mol^{-1})	$\Delta G^{\ddagger 0}$ (kJ mol^{-1})	Rate Constant (k)	Unit of k
1	**Fe + tBuOOH → Fe-tBuOOH**	16	66[a]	$2.65*10^{1}$	Lmol^{-1}s^{-1}
2	**Fe-tBOOH → Fe-OH + $tBuO\cdot$**	-48	5	$9.53*10^{11}$	s^{-1}
3	**Fe-OH + tBuOH → Fe-tBuOO + H_2O**	-45	61	$1.95*10^{2}$	Lmol^{-1}s^{-1}
4	**Fe-tBuOO → Fe=O + $tBuO\cdot$**	-1	66[a]	$2.65*10^{1}$	Lmol^{-1}s^{-1}
5	**Cy_HH + $tBuO\cdot$ → $Cy^{\cdot}_{H}$ + tBuOH**	-47	41	$5.19*10^{5}$	Lmol^{-1}s^{-1}
6	**$Cy^{\cdot}_{H}$ + $tBuO\cdot$ → Cy: + tBuOH**	5	46	$6.12*10^{4}$	Lmol^{-1}s^{-1}
7	**Fe-OH + $Cy^{\cdot}_{H}$ → Fe-Cy_HOH**	-135	66[a]	$2.65*10^{1}$	Lmol^{-1}s^{-1}
8	**Fe-Cy_HOH → Fe + Cy_HOH**	-1	66[a]	$2.65*10^{1}$	Lmol^{-1}s^{-1}
9	**Fe=O + Cy: → Fe-CyO**	-414	66[a]	$2.65*10^{1}$	Lmol^{-1}s^{-1}
10	**Fe-CyO → Fe + CyO**	4	66[a]	$2.65*10^{1}$	Lmol^{-1}s^{-1}
11	**Fe=O + Cy_HOH → Fe-OH + $Cy^{\cdot}_{OH}$**	61	85	$1.71*10^{-2}$	Lmol^{-1}s^{-1}
12	**Fe-OH + $Cy^{\cdot}_{OH}$ → Fe-Cy_{OH}OH**	-124	66[a]	$2.65*10^{1}$	Lmol^{-1}s^{-1}
13	**Fe-Cy_{OH}OH → Fe+ CyO + H_2O**	-70	66[a]	$2.65*10^{1}$	s^{-1}

[a] Step without activation energy barrier; activation Gibbs free energy was calculated as a sum of the entropic contribution and an estimate of the free energy barrier of diffusion. See "Computational Methods' section of the main text for full details.

$\Delta G^{\ddagger 0}$refers to activation Gibbs free energy in standard state (c = 1 mol dm^{-3} for the transition state and the reactant(s)), which equals to $\Delta G^{\ddagger}$ in the case of unimolecular reactions, while $\Delta G^{\ddagger}$ - 7.93 kJ mol^{-1} in the case of bimolecular reactions. k values were obtained from $\Delta G^{\ddagger 0}$ using the Eyring-Polányi equation, as described in the "Computational Methods" section of our paper. An initial concentration of 1×10^{-7} mol L^{-1} for the catalyst was used for the MKM and this was estimated based on the reported metal wt% in Table 1 of the main text, and the amount of catalyst added to the reaction solution (0.020 g_{cat} in 4 cm^3 of solution).

Table S.4. Sensitivity coefficient of cyclohexanol and cyclohexanone production rate to the rate constants of elementary steps considered in our MKM. The sensitivity coefficient is show for steps with a calculated DFT barrier only.

Step Number	Elementary step	-ol Sensitivity Coefficient	-one Sensitivity Coefficient
1	Fe + tBuOOH → Fe-tBuOOH	-	-
2	Fe-tBOOH → Fe-OH + $tBuO\cdot$	0.00	0.00
3	Fe-OH + tBuOH → M-tBuOO + H_2O	-0.99	0.00
4	Fe-tBuOO → Fe=O + $tBuO\cdot$	-	-
5	Cy_HH + $tBuO\cdot$ → $Cy^{\cdot}_H$ + tBuOH	0.00	-0.99
6	$Cy^{\cdot}_H$ + $tBuO\cdot$ → Cy: + tBuOH	0.00	1.00
7	Fe-OH + $Cy^{\cdot}_H$ → Fe-Cy_HOH	-	-
8	Fe-Cy_HOH → Fe + Cy_HOH	-	-
9	Fe=O + Cy: → Fe-CyO	-	-
10	Fe-CyO → Fe + CyO	-	-
11	Fe=O + Cy_HOH → Fe-OH + $Cy^{\cdot}_{OH}$	-0.74	0.00
12	Fe-OH + $Cy^{\cdot}_{OH}$ → Fe-Cy_{OH}OH	-	-
13	Fe-Cy_{OH}OH → Fe+ CyO + H_2O	-	-

Table S.5. List of elementary steps and their corresponding degree of selectivity control (X_{SC})

Step Number	**Elementary Step**	**X_{SC}**
1	**Fe + tBuOOH → Fe-tBuOOH**	**0**
2	**Fe-tBOOH → Fe-OH + $tBuO\cdot$**	**0**
3	**Fe-OH + tBuOH → Fe-tBuOO + H_2O**	**-1.0**
4	**Fe-tBuOO → Fe=O + $tBuO\cdot$**	**0**
5	**Cy_HH + $tBuO\cdot$ → $\dot{Cy}_H$ + tBuOH**	**1.0**
6	**$\dot{Cy}_H$ + $tBuO\cdot$ → Cy: + tBuOH**	**-0.5**
7	**Fe-OH + $\dot{Cy}_H$ → Fe-Cy_HOH**	**0**
8	**Fe-Cy_HOH → Fe + Cy_HOH**	**0**
9	**Fe=O + Cy: → Fe-CyO**	**0**
10	**Fe-CyO → Fe + CyO**	**0**
11	**Fe=O + Cy_HOH → Fe-OH + $\dot{Cy}_{OH}$**	**0**
12	**Fe-OH + $\dot{Cy}_{OH}$ → Fe-Cy_{OH}OH**	**0**
13	**Fe-Cy_{OH}OH → Fe+ CyO + H_2O**	**0**

S.13.1 Additional Microkinetic Modeling Discussion

To validate our approximation of the rate of barrierless elementary steps, we also estimated the rates of the barrierless steps using collision theory as suggested by previous studies involving zeolite catalysis.[7-9] Adsorption and desorption rate constants were modeled using collision theory as follows:

$$k_{ads/des} = \frac{\sigma A}{\sqrt{2\pi m k_B T}} \qquad \text{(S.14)}$$

where σ is the sticking coefficient, A is the site area, m is the molar mass of the adsorbate. We adopted a value of σ=1 and A=1 × 10^{-18} m^2.[7-9] As shown in Figure S.28 below, the microkinetic model with the rates of barrierless steps estimated using collision theory (Table S.3) provides results which are inconsistent with the experimental results. The model predicts that cyclohexanol is the main product of the reaction (Figure S.28, left), with a selectivity of 90% after 8000 seconds

(Figure S.28, right). Thus, we conclude that collision theory does not properly capture the rates of barrierless elementary steps as it does not incorporate the effects of the solvent. “

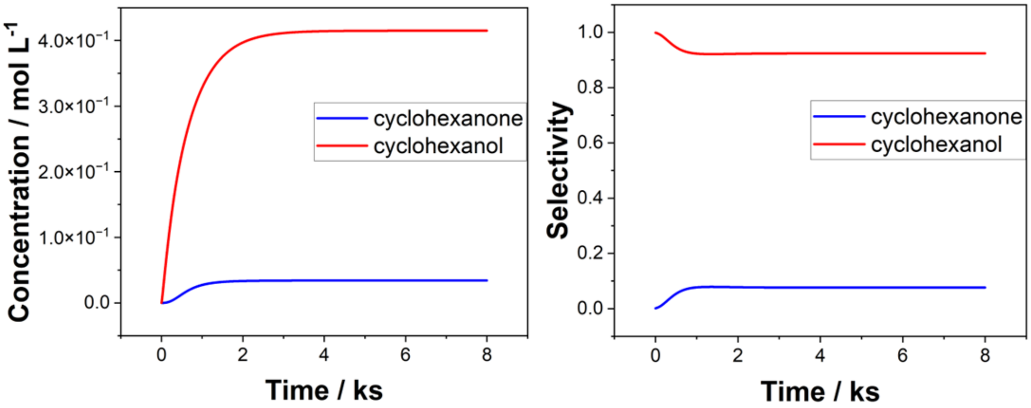

Figure S.28. Concentration of cyclohexanol and cyclohexanone as a function of time (left) and selectivity of cyclohexanol and cyclohexanone as a function of reaction time (right) from microkinetic modeling studies whereby the rates of the barrierless elementary steps were estimated using collision theory.

S.14 References

1. P. B. Weisz and C. D. Prater, *Advances in Catalysis*, 1954, **6**, 143-196.
2. J. A. Atias and H. de Lasa, *Chemical Engineering Science*, 2004, **59**, 5663-5669.
3. N. Koone, Y. Shao and T. W. Zerda, *The Journal of Physical Chemistry*, 1995, **99**, 16976-16981.
4. B. Taylor, J. Lauterbach, G. E. Blau and W. N. Delgass, *Journal of Catalysis*, 2006, **242**, 142-152.

5. R. F. Parton, P. E. Neys, P. A. Jacobs, R. C. Sosa and P. G. Rouxhet, *Journal of Catalysis*, 1996, **164**, 341-346.
6. J.-A. Becerra, L.-M. González and A.-L. Villa, *Journal of Molecular Catalysis A: Chemical*, 2016, **423**, 12-21.
7. G. Gupta and B. C. Bukowski, *The Journal of Physical Chemistry C*, 2024, **128**, 20104-20117.
8. B. C. Bukowski, J. S. Bates, R. Gounder and J. Greeley, *Journal of Catalysis*, 2018, **365**, 261-276.
9. J. S. Bates, B. C. Bukowski, J. W. Harris, J. Greeley and R. Gounder, *ACS Catalysis*, 2019, **9**, 6146-6168.